

To appear in the Sept. 2001 issue of The Astronomical Journal

Multimetric Observations of the Center of M 81 : A Starved Nucleus with Intraday Variability

Kazushi Sakamoto^{1,2}, Hiroyuki Fukuda³, Keiichi Wada³, and Aso Haba⁴

ABSTRACT

The central kiloparsec of M 81 has been observed in the CO ($J=1\{0$) line and the 3 mm continuum at 100 pc resolution in an attempt to probe molecular gas, and to search for the nuclear inner Lindblad resonance (N ILR), around the low-luminosity AGN M 81. We found the following. (1) Molecular gas in the central kpc is mainly on a "pseudoring" or a spiral arm at a radius of about 500 pc. (2) The region within 300 pc from the nucleus is mostly devoid of molecular gas except for dust; in particular, there is neither a giant molecular cloud that is now accreting on the nucleus nor a conspicuous gas feature that can be identified as an N ILR. (3) The 3 mm continuum emission shows significant intraday variation, suggesting an emitting region of ~ 100 AU. (4) The 3 upper limit for CO absorption toward the continuum source is $\tau_{\text{CO}(0\{1)} dV < 0.1$ for a linewidth of 10 km s^{-1} . The dearth of accreting molecular gas in the vicinity of the nucleus may explain the low luminosity of M 81.

Subject headings: galaxies: active | galaxies: individual (M 81, NGC 3031) | galaxies: ISM | galaxies: kinematics and dynamics | galaxies: spiral

1. Introduction

M 81 is a large ($L_B = 2 \times 10^{10} L_\odot$; Tully 1988), early-type (SA(s)b; de Vaucouleurs et al. 1991), spiral galaxy at a distance of 3.6 Mpc (Freedman et al. 1994). At the center of M 81 is an AGN called M 81, for which an accreting massive black hole has been indicated by, among other things, a power-law X-ray continuum, a broad H β line, a compact core-jet structure in radio wavelengths, and rapid variability of these features (Ishisaki et al. 1996; Bartel & Bietenholz 2000;

¹Nobeyama Radio Observatory, Minamisanaka, Nagano, 384-1305, Japan

²Harvard-Smithsonian Center for Astrophysics, Submillimeter Array, P. O. Box 824, Hilo, HI 96721, E-mail: ksakamoto@cfa.harvard.edu

³National Astronomical Observatory, Mitaka, Tokyo, 181-8588, Japan

⁴Department of Physics, Hokkaido University, Sapporo, 060-0810, Japan

Bower et al. 1996, and references therein). In fact, M 81 is one of the nearest galaxies that host an AGN with such strong evidence. The luminosity of the nucleus, $L_{2-10\text{keV}} \approx 2 \times 10^{40} \text{ erg s}^{-1}$, $L_{\text{H}} \approx 4 \times 10^7 \text{ erg s}^{-1}$, and $L_{6\text{cm}} \approx 1 \times 10^{30} \text{ W Hz}^{-1} \text{ str}^{-1}$, places it among the low-luminosity AGN (Ishisaki et al. 1996; Ho, Filippenko, & Sargent 1997; de Bruyn et al. 1976).

An interesting issue that can be addressed from observations of molecular gas around M 81 is fueling to the active nucleus; e.g., whether the low-luminosity AGN is suffering from a shortage of fuel. Also related to this issue is the search for the nuclear inner Lindblad resonance (NILR)⁵ that is predicted to form around a central massive black hole and help fuel it (Fukuda, Wada, & Habe 1998; Fukuda, Habe, & Wada 2000, hereafter referred to as FWH98 and FWH00, respectively). The proximity of M 81 and the estimated mass of the central black hole, ranging from $(3\text{--}8) \times 10^5 M_{\odot}$ to $> 4 \times 10^7 M_{\odot}$ (Filippenko & Sargent 1988; Iyomoto & Makishima 2001, and references therein) provide a good chance to detect the NILR. Conveniently, M 81 has a small nuclear bar of $\sim 1 \text{ kpc}$ length that could drive the resonance (Elmegreen, Chromey, & Johnson 1995; Reichen et al. 1994). In addition, millimeter continuum emission from M 81, which is strong thanks to the galaxy's proximity, allows us to probe the tenuous molecular gas in front of the nucleus through absorption studies. Further, monitoring the millimeter continuum during observations tells us the variability of M 81.

CO emission from cold molecular gas in the center of M 81 was first detected by Sage & Westpfahl (1991) using the NRAO 12 m telescope. No further observation has been reported, and, hence, the distribution of molecular gas around the nucleus has not been known to better than 1 kpc resolution. Millimeter continuum emission from M 81 was detected once by Reuter & Lesch (1996) but no monitoring has been reported.

We observed the central kpc ($1''$) of M 81 at $\sim 100 \text{ pc}$ resolution in CO ($J=1\{0\}$) line and 3 mm continuum using the Nobeyama Millimeter Array (NMA). The data revealed, for the first time, the distribution of molecular gas in the vicinity of the nucleus, served as a monitor of the continuum emission from M 81 with a time resolution of $\sim 30 \text{ min}$, and also allowed us to search for cold molecular gas in front of the nucleus through absorption.

2. Observations and Data Reduction

We observed the CO ($J=1\{0\}$) line and 3 mm continuum using the NMA from November 1999 to January 2000 and in April 2000. The six 10 m telescopes of the array are equipped with SIS receivers of single polarization and have $1''$ beam size in FWHM. They were pointed toward M 81 at $\text{B}_{1950} = 9^{\text{h}}51^{\text{m}}27^{\text{s}}.3004$ and $\text{B}_{1950} = +69^{\circ}18'08''.267$ (Ma et al. 1998). The log of observations is

⁵The name of the resonance was "nuclear Lindblad resonance (NLR)" when it was first proposed. However, we rename it in this paper to avoid confusion with the "narrow line region" whose widely-used acronym in AGN studies is also NLR. The new name also makes it clear that the resonance is an inner Lindblad resonance (see x4).

in Table 1. We obtained seven transits in the most compact D configuration and one in the sparse AB configuration. Two sets of correlators, UWBC and FX, were used simultaneously, with UWBC covering 512 MHz (1300 km s^{-1} for CO) with 256 channels and FX covering 32 MHz (80 km s^{-1} for CO) with 1024 channels. This setup was used to observe the broad CO emission line ($V = 400 \text{ km s}^{-1}$) and to search for a narrow absorption line of CO against the continuum emission from M 81. The CO line was observed in the upper sideband (USB) at 115 GHz, while continuum data were obtained from the lower sideband (LSB) at 103 GHz, where the atmospheric attenuation is less severe. Data from both sidebands were recorded in every 8 sec; this high rate was employed to reduce coherence loss in the measurements of continuum flux density. In each transit, M 81 and a quasar B0836+710, which is 6" away from M 81, were observed in 20- or 30-min cycles, and either 3C273 or 3C279 was observed for 30 min for passband calibration. Atmospheric attenuation was corrected by the chopper-wheel method. Flux scale was established by comparing quasars with Uranus. The flux density of the calibrator B0836+710 was measured a total of 14 times during our observations. It was 1.4 Jy in the first session of observations from November through January and 1.6 Jy in the second session in April, being constant during each session, with about 10% error.

Maps of CO emission were made using standard data-reduction techniques for radio interferometry, including gain and passband calibration as well as continuum subtraction in UVPROC2, and Fourier transform and deconvolution in AIPS. Data from the AB configuration were not used to make maps of CO emission, because little emission was detected in long baselines. Resulting CO maps have a resolution of $6''.9 \times 5''.8$ ($\theta_{PA} = 36^\circ$), which corresponds to $120 \times 100 \text{ pc}$ at the distance of the galaxy. The maps in this paper are not corrected for the primary beam response, but all flux measurements have been corrected for it.

Absorption of CO has been searched in both UWBC and FX data. UWBC data were binned every 2 channels to obtain 4 MHz (10.4 km s^{-1}) resolution, while FX data were binned every 16 channels to obtain 0.5 MHz (1.3 km s^{-1}) resolution. Flux density of the nucleus was measured in each channel of the data cubes that were made without continuum subtraction, and provided spectra of the central 100 pc of M 81. Linear baseline was subtracted from each spectrum, to cancel small differences in spectral index between M 81 and the passband calibrators. The rms of each spectrum is 0.032 and 0.14 for UWBC and FX spectrum, respectively, in the unit where the flux density of M 81 is unity.

Variations in M 81 were monitored using the LSB data. The LSB data were first averaged over the 512 MHz band, and then averaged over the 20- or 30-min of time between gain calibrator observations. The latter averaging was made for visibility amplitudes to avoid coherence loss. Arithmetic averaging of amplitudes (so-called 'scalar averaging') was used when the signal-to-noise ratio of each visibility was high enough (> 7), and the maximum likelihood method was used when it was not, thus avoiding bias due to amplitude averaging. The LSB data for B0836+710 were reduced in the same way, and used to remove any variation in system and atmospheric conditions. The use of B0836+710 as a gain calibrator here, as well as in the mapping above, has a built-in assumption that it had a constant flux density and was unpolarized during each transit. We believe the assumption

is found as discussed below.

3. Results

3.1. CO emission

Figures 1 and 2 show CO channel maps and the integrated intensity map, respectively. The CO emission is greater than 3 mJy beam^{-1} from 187 km s^{-1} to 146 km s^{-1} , with nondetection in two channels near the systemic velocity. The velocity range, as well as the depression near the systemic velocity, is in good agreement with the previous single-dish observations. It is evident in the maps that CO emission is seen around the galactic center, mostly at galactocentric radii of between 300 and 600 pc. The gas distribution is lopsided, and little emission is seen to the west of the nucleus. For simplicity, we call the overall structure a "pseudoring" at a galactocentric distance of about 500 pc, though our data do not rule out other descriptions for the structure, such as spiral arm(s). In fact, a somewhat similar structure in H₂ was called "nuclear spiral" in Devereux et al. (1995). The pseudoring has a peak molecular gas surface density $120 \text{ M}_{\odot} \text{ pc}^{-2}$ at our resolution, where no correction for inclination has been made, and the following Galactic CO-to-H₂ conversion relation is assumed (Scoville et al. 1987; Solomon et al. 1987; Strong et al. 1988):

$$\frac{M_{\text{mol}}}{\text{M}_{\odot} \text{ pc}^2} = 6.8 \times 10^2 \frac{I_{\text{CO}}}{\text{Jy km s}^{-1} \text{ arcsec}^2} : \quad (1)$$

The total mass of molecular gas in the pseudoring is $1 \times 10^7 \text{ M}_{\odot}$, and the structure is apparently made of several gas clumps. The peak brightness temperature of each clump is 0.3 K when averaged over our beam size of 100 pc and a velocity width of 21 km s^{-1} , comparable to those for giant molecular clouds (GMCs) and GMC complexes in the outer regions of M 81 (Taylor & Wilson 1998; Rouillet et al. 1998). It is also notable that the nucleus is devoid of CO emission. The closest components to the nucleus are the GMCs seen in the -124 , -104 , and $+42 \text{ km s}^{-1}$ maps at the deprojected galactocentric radius of 300 pc . Their masses are $M_{\text{mol}} \approx 5 \times 10^5 \text{ M}_{\odot}$.

Figure 3 is the CO spectrum observed with NMA, whose primary beam is $60''$ in FWHM. The total CO flux is 50 Jy km s^{-1} , which is half the single-dish flux observed with the NRAO 12 m telescope in its $55''$ beam (Sage & Westpfahl 1991). Thus, provided that calibrations are accurate in both observations, we recovered about half the total CO flux; the rest must be either too extended or too faint (or both) to be detected with our interferometric observations. If the missed emission is uniformly distributed in our field of view and has a linewidth of 20 km s^{-1} or smaller at each position, then its intensity in our channel maps would be 28 mJy beam^{-1} , while the rms in the channel maps is 13 mJy beam^{-1} . It thus seems more likely that the missing flux is mainly due to a smoothly distributed population of small molecular clouds in the central kiloparsec. Widespread distribution of small clouds, in addition to larger GMCs, has been suggested also on a spiral arm of M 81 (Rouillet et al. 1998).

The overall rotation seen in the channel maps is largely consistent with what is expected from the moderately inclined ($i = 58^\circ$) galaxy whose receding major axis is at $P.A. = 330^\circ$ (Adler & Westpfahl 1996). Detailed velocity field structure is hard to discern in the limited spatial coverage of the current data, but obvious noncircular motions are not seen. The CO linewidth of 350 km s^{-1} is already attained at a radius of $30''$, while the linewidth of HI peaks at about 420 km s^{-1} at a radius of $400''$ (Adler & Westpfahl 1996). If the inner CO and outer HI disks are coplanar and neither of them is affected by noncircular motions, then the rotation curve of M 81 reaches 80% of its maximum already at a radius of 500 pc. If the above assumptions hold, then the rotation curve is steeper in the central regions than estimated from previous HI observations (Fig. 7 of Adler & Westpfahl 1996), but is consistent with ones observed in spiral galaxies of similar luminosity (Sakamoto et al. 1999a). This is not surprising considering the lower spatial resolution of the HI observations. The Keplerian dynamical mass calculated from the CO linewidth is $M_{\text{dyn}}(r = 500 \text{ pc}) = 1 \times 10^9 M_\odot$.

The active nucleus M 81 appears to be very close to the dynamical center of the galaxy; a conservative upper limit to the offset is $10''$ or 200 pc. Thus M 81 is not significantly displaced from the dynamical center despite its small mass, which Ho, Filippenko, & Sargent (1996) estimated to be $0.7 \times 10^6 M_\odot$ comparable to that of a GMC complex.

3.2. Continuum emission

Continuum emission is detected only from the nucleus, and its flux density varied during our observations. Figure 4 shows amplitudes of M 81 and 0836+710 during observations on 2000 January 1 and 3. The upper panels show data before the gain calibration using 0836+710 but after the chopper-wheel calibration. The data taken in better weather on January 1 show that the amplitude of 0836+710 was constant to $\pm 5\%$ during the 6-hr observations, in which the parallactic angle of the source changed almost linearly by 100° . The amplitude should have varied sinusoidally if the source was linearly polarized, because we observed in linear polarization mode with position angle rotating with the parallactic angle. The constant amplitude suggests that 0836+710 had a constant flux density and a negligible degree of linear polarization, unless 0836+710 varied to compensate for polarization, which is unlikely. We also did not see significant variation in the amplitude of 0836+710 during observations made on other dates in stable weather conditions.

The lower panels in Fig. 4 show data after gain calibration, in which a gain curve is obtained by interpolating the amplitude of 0836+710 with a Gaussian kernel that has $\sigma = 0.015$ day and a cutoff at $t = 0.050$ day. The gain calibration is necessary and useful, especially for data taken in changing weather conditions, such as those on January 3. The common variation seen in the two sources on that date must be mostly due to varying radio seeing and coherence loss, judging from the correlation between the amplitudes and the scatter in visibility phases. After the gain calibration, the amplitude of M 81 shows almost linear variation on both dates. The lack of a sinusoidal pattern suggests that the linear polarization of M 81 is not large enough to dominate

the amplitude variation, and that the amplitude variation is mainly due to the variation of the total flux density of M 81.

Table 2 lists the flux density of M 81 and its rate of variation for each night. The most important result is that M 81 varies in almost every track of duration 5{10 hrs by a few to several 10 %. In particular, M 81 appears to have had a flare on JD = 2451456, as shown in Fig. 5. During our observing period of 152 days, the ratio of the maximum to the minimum flux density is 7, and the mean flux density is 0.39 Jy, a factor of 2 larger than the only previous measurement (at 3.4 mm) made in 1993 by Reuter & Lesch (1996). It is also notable that variability is almost linear in each day and that we do not see significant variation with timescales of a few hours or less, even though the resolution of our observations is 0.5 hrs.

To characterize the timescale of the variation, doubling time is calculated as the time in which M 81 would have varied by a factor of 2 if it had held its linear trend in variation in each track. We do this extrapolation because M 81 did not show two-fold variation in any single track. The largest variation seen in a single track is the 45% increase during the 0.24-day observations on January 1. The doubling timescales defined this way are 1 day, as listed in Table 2. Also, flux density (without extrapolation) doubled in 1.2 days during our first 2 days of observations. Thus M 81 has intraday variability at 3 mm.

The variation of radio emission from M 81 has long been known in centimeter wavelengths (Crane et al. 1976; de Bruyn et al. 1976; Ho et al. 1999; Bietenholz et al. 2000), with the degree of variation being about a factor of 2 over years and being smaller in longer wavelengths. Although 40% variation in 4 days was observed in 1974 by Crane et al. (1976), recent extensive observations did not agree on the variation in short timescales (days). While Ho et al. (1999) reported 10{60 % variation on the timescale of .1 day at 3.6 cm, Bietenholz et al. (2000) did not see variations larger than their 5% standard error in their 12 epochs of 12{18 hr observations at the same wavelength. Our observations show that intraday variability does exist at a millimeter wavelength. The larger degree of variation (a factor of 7 in our observing period of 5 months) is in accordance with the trend that the degree of variation increases with frequency.

The size scale of the millimeter-emitting region should be below about 1 light-day or a few 100 AU from the light-crossing time argument, if there is no relativistic beaming. This size is consistent with what is extrapolated from VLBI observations in centimeter wavelengths, where the size is 700 AU in 22 GHz and changes with frequency as $\nu^{-0.8}$ between 2.3 and 22 GHz (Bietenholz et al. 1996). It is also comparable to the size of the broad-line region in this galaxy (Filippenko & Sargent 1988; Ho, Filippenko, & Sargent 1996). For a source 1 light-day or smaller, the brightness temperature needs to be greater than 10^{11} K at 3 mm in order to have a flux density of 1 Jy. The 3 mm emission from M 81 is obviously nonthermal, as is the case with the centimeter emission, and the high brightness temperature is comparable to those observed in the cores of radio galaxies.

3.3. CO absorption

Figure 6 shows spectra of M 81, at high- and low-velocity resolutions, in the frequencies where CO (0-1) absorption would be caused by molecular gas in either M 81 or the Galaxy or both. No absorption is seen in the spectra. The 3- σ upper limit of the CO optical depth is 0.1 and 0.5 for linewidths of 10.4 km s⁻¹ and 1.3 km s⁻¹, respectively.

Hydrogen column density toward M 81 has been estimated from X-ray observations to be $N_H \sim 1 \times 10^{21}$ cm⁻² (Ishikawa et al. 1996; Pellegrini et al. 2000). If the absorbing material is mostly molecular gas with a CO abundance of $[CO]/[H_2] = 10^{-4}$, then the integrated optical depth of CO, $\int \tau_{CO(0-1)} dV$, would be 10 and 1 km s⁻¹ for LTE temperatures of 10 and 30 K, respectively. The CO absorption should have been detected in the case of lower temperature gas. Possible reasons for the nondetection therefore include ionized or atomic absorbing material, low CO abundance, high temperature (> 30 K) of molecular gas, and a large velocity width of the absorbing gas.

4. Search for the Nuclear Inner Lindblad Resonance

Nuclear inner Lindblad resonance is the resonance between perturbations from a stellar bar and epicyclic motion of gas clouds orbiting around the galactic center that hosts a central massive black hole (FWH98). It is formed, like other inner Lindblad resonances, on the radius at which $\Omega = 2\kappa$ is equal to Ω_{bar} , where Ω is angular frequency of the orbiting clouds, κ is the epicyclic frequency, and Ω_{bar} is the pattern speed of the bar. Figure 7 shows a model rotation curve and its $\Omega = 2\kappa$ in a potential with a central massive black hole. It is the upturn of the rotation curve toward the central black hole that causes the upturn of the $\Omega = 2\kappa$ curve and makes the NILR possible. As seen below, the dynamical effect of a central massive black hole is far-reaching, being able to form the NILR even at a radius within which only 1% of the total mass is due to the black hole.

4.1. Maximum Radius of NILR

The maximum radius at which an NILR can be formed is where $\Omega = 2\kappa$ is its minimum⁶. This radius, $\text{max}(R_{\text{NILR}})$, is expected to be closely related to the radius where the rotation curve hits its minimum. We call the latter radius nuclear turnover and denote it as R_{nt} . The nuclear turnover, R_{nt} , is observable and can be easily understood as the radius where the mass of the central black hole is comparable to the mass of the other components inside it. For these reasons, R_{nt} must be a good scale to measure $\text{max}(R_{\text{NILR}})$. In fact, there are cases where the ratio of the two radii,

⁶This is also the minimum radius at which the inner inner Lindblad resonance (IILR) can form. The two resonances can degenerate at this radius.

$\max(R_{\text{N ILR}}) = R_{\text{nt}}$, can be related to the relative mass of the central black hole with respect to the characteristic mass within the ordinary turnover radius of the rotation curve.

The rotation curve of a galaxy with a central massive black hole can be written, when normalized, in the form

$$v_{\text{total}}(r) = \sqrt{v_g^2(r) + \frac{m}{r}}; \quad (2)$$

where r and v are normalized radius and velocity, respectively, $v_g(r)$ is the normalized rotation curve of the galaxy without the central black hole, and m is the normalized mass of the black hole. It is assumed that the galaxy is not strongly barred. We normalize radius so that the turnover radius of the rotation curve $v_g(r)$ is at $r = 1$ and normalize the velocity so that the flat (or peak) rotation velocity is $v = 1$. Consequently, the parameter m is roughly the ratio of the black hole mass to the galaxy mass within the turnover radius and should satisfy $m \ll 1$ for most disk galaxies.

Let us consider the case where the rotation curve without the central black hole can be well approximated, from the center through the turnover radius, with the first few terms of the Taylor-expansion,

$$v_g(r) = ar + br^2 + cr^3 + \dots; \quad (3)$$

The coefficient a is positive and of the order of unity, and the first non-zero coefficient after a is negative and is also of the order of unity. An example of this class is the rotation curve of the logarithmic potential,

$$v_{g;\log}(r) = \sqrt{\frac{r}{1+r^2}} \quad (4)$$

$$= r - \frac{1}{2}r^3 + \dots; \quad (5)$$

where $a = 1$, $b = 0$, and $c = -1/2$. The radius of nuclear turnover is, for small m ,

$$r_{\text{nt}} = \frac{m}{2a^2}^{1/3}; \quad (6)$$

The maximum radius of the nuclear inner Lindblad resonance is, from the minimum of the curve,

$$\max(r_{\text{N ILR}}) = \frac{9m}{2ab}^{1/4} \quad (7)$$

if b is not zero. It is

$$\max(r_{\text{N ILR}}) = \frac{9m}{8ac}^{1/5} \quad (8)$$

if b is zero but c is not. The ratio of the two radii is, therefore,

$$\frac{\max(r_{\text{N ILR}})}{r_{\text{nt}}} = \begin{cases} 1.8 m^{1/12} a^{5/12} (|b|)^{1/4} & \text{if } b \neq 0 \\ 1.3 m^{2/15} a^{7/15} (|c|)^{1/5} & \text{if } b = 0 \text{ and } c \neq 0 \end{cases} \quad (9)$$

Ignoring the coefficients a, b, c , which are of the order of unity, the ratio is in the range of 2-8 for the fractional mass range of $m = 10^{-2} \text{ } \{ 10^{-6}$. The weak dependence of $m_{\text{ax}}(r_{\text{N ILR}})$ on the black hole mass m is notable, and the nearly constant value of the $m_{\text{ax}}(r_{\text{N ILR}}) = r_{\text{nt}}$ for the most realistic range of m ensures that r_K can be conveniently used to measure the radius of the N ILR.

There are rotation curves for which Taylor expansion is not possible around $r = 0$ and therefore the above analysis does not apply. However, some of those rotation curves do have similar characteristics on N ILR as in the cases discussed above. An example is the rotation curve of an exponential disk with surface density $\Sigma(R) = \Sigma_0 \exp(-R/R_d)$,

$$v_{g,\text{exp}}(r) = 2^{3/2} r [I_0(r)K_0(r) - I_1(r)K_1(r)]^{1/2}; \quad (10)$$

where the radius is normalized as $r = R/2R_d$, and I and K are modified Bessel functions (see Binney & Tremaine (1987) p.77). The turnover radius of the rotation curve is $r = 1.1$. The conditions that approximately describe r_{nt} and $m_{\text{ax}}(r_{\text{N ILR}})$ are, for small m ,

$$r_{\text{nt},\text{exp}}^3 (\log r_{\text{nt},\text{exp}}) = \frac{m}{16} \quad (11)$$

and

$$[m_{\text{ax}}(r_{\text{N ILR},\text{exp}})]^3 (\log r_{\text{N ILR},\text{exp}})^{-1} = \frac{9m}{4}; \quad (12)$$

respectively. They lead to the formula

$$\frac{m_{\text{ax}}(r_{\text{N ILR},\text{exp}})}{r_{\text{nt},\text{exp}}} = f 36 \log [m_{\text{ax}}(r_{\text{N ILR},\text{exp}})] \log r_{\text{nt},\text{exp}} g^{1/3} \quad (13)$$

that shows the ratio being larger for smaller m but being very weakly dependent on m , as is the case for eq. (9). Numerically, the ratio is in the range of 5-9 for $m = 10^{-2} \text{ } \{ 10^{-6}$.

The parameter m for M 81 is estimated to be $m = 5 \times 10^5 \text{ } \{ 5 \times 10^3$, by use of $M_{\text{dyn}}(r = 500 \text{ pc}) = 1 \times 10^{10} M_{\odot}$ obtained from our CO observations and the black hole mass in the literature (see x1). For this range of m , as we have seen, N ILR can be formed at up to several times larger radius than the nuclear turnover. The nuclear turnover radius, R_{nt} , can be constrained as $R_{\text{nt}} = 15 \text{ } \{ 70 \text{ pc}$ by using the assumption that the mass density is uniform in the central kpc. It is an upper limit because the density most likely increases toward the galactic center, as readily inferred from light distribution. Combining these numbers, we can estimate $m_{\text{ax}}(R_{\text{N ILR}})$ to be 100 pc for a smaller number for the black hole mass and 300 pc for a larger number. Thus it is unlikely that the gas feature (pseudoring) at around 500 pc is due to an N ILR. Note that the radius of an N ILR can be much smaller than the upper limits (and R_{nt}) for a large bar .

4.2. Numerical Simulations

We made numerical simulations for gas around an N ILR by using parameters adjusted for M 81 in order to tell what can be seen if there is an N ILR in the galaxy. The simulation is non-selfgravitating, isothermal, and two-dimensional. Evolution of a rotating gas disk is simulated in a

{ 10 {

time-independent, external potential having a bar and a central black hole. The potential is in the form

$$\Phi_{\text{ext}} = \Phi_{\text{BH}} + \Phi_{\text{bar}} + \Phi_{\text{disk}}; \quad (14)$$

where Φ_{BH} , Φ_{bar} , and Φ_{disk} are a central massive black hole, a stellar bar, and a disk, respectively. They are defined as follows:

$$\Phi_{\text{BH}}(R) = \frac{GM_{\text{BH}}}{(R^2 + a^2)^{1/2}}; \quad (15)$$

$$\Phi_{\text{disk}}(R) = \frac{3^{3/2}}{2} \frac{a_d v_0^2}{(R^2 + a_d^2)^{1/2}}; \quad (16)$$

and

$$\Phi_{\text{bar}}(R; \theta) = \frac{3^{3/2}}{2} \frac{a_b v_0^2}{(R^2 + a_b^2)^{1/2}} \left[1 + \epsilon_0 \frac{a_b R^2}{(R^2 + a_b^2)^{3/2}} \cos 2\theta \right]; \quad (17)$$

with $a = 10$ pc, $a_d = 5$ kpc, $a_b = 0.5$ kpc, $v_0 = 200$ km s⁻¹, and $\epsilon_0 = 0.05$. This model is based on the potentials used in Wada, Minezaki, & Sakamoto (1998). Figure 7 shows the rotation curve and $\Phi = 2$ of the model potential with $M_{\text{BH}} = 10^7 M_\odot$. The initial gas disk is axisymmetric and rotationally supported, with a uniform surface density and total mass of $10^7 M_\odot$ within a 2 kpc diameter. The isothermal equation of state is adopted along with a sound velocity of 10 km s⁻¹.

We use the second-order Euler mesh code, which is based on the Advection Upstream Splitting Method (AUSM; Liou & Steen 1993), to solve the hydrodynamical equations. Details of the numerical scheme are described in Wada & Norman (2001). Simulations are made on 512 × 512 Cartesian grid points in a region of 2 × 2 kpc; the spatial resolution is 3.9 pc.

Figure 8 shows time evolution of gas for $v_{\text{bar}} = 50$ km s⁻¹ kpc⁻¹ and $M_{\text{BH}} = 10^6, 10^7$, and $10^8 M_\odot$. Table 3 lists R_{nt} , R_{NILR} , and $\max(R_{\text{NILR}})$ for each mass of the black hole. The small concentration of gas that develops near the galactic center at $R \approx R_{\text{NILR}}$ is due to the NILR. The two-armed spiral structure is more clearly seen in cases with larger M_{BH} . Evolution of gas around an NILR, especially when the self-gravity of gas is important, has been studied in more detail in FHW00 and in FWH98. Outside NILR, the inner inner Lindblad resonance (ILR) creates an oval-shaped gas distribution, two leading spirals, with its major axis leading the bar major axis by about 45°.

4.3. Comparison with Observations

The lack of CO emission around the nucleus, inside the 500 pc pseudoring, prevents us from detecting the features of an NILR. Among the reasons that can possibly explain the absence of these features are the following: 1) the NILR had quickly driven most of gas around the nucleus to the AGN as suggested in FWH00; 2) the gas around the NILR is not in molecular form; 3) the NILR is at a too small radius for us to detect the gas accumulated around the resonance; and 4) the NILR does not exist because of a slow pattern speed or weakness of the bar perturbation. Despite

the nondetection in CO, HST images in optical revealed a spiral dust lane extending $12''$ (200 pc) to the north of the nucleus, and a disk-like feature of $7''$ (120 pc) diameter in H α (D'evereux, Ford, & Jacoby 1997; Pogge et al. 2000). These features could be related to an N ILR. Kinematical information is needed to confirm the possibility.

The pseudoring (or spiral feature) in molecular gas at $R \approx 500$ pc is suggestive of a gas dynamical mechanism to arrange gas clouds — possibly an inner Lindblad resonance. The current data, however, are too scarce to pinpoint the mechanism, other than to say that it is unlikely to be an N ILR. The dynamics in the central kiloparsec may well be affected by the nuclear bar, or oval distortion, seen in the near-infrared, whose semimajor axis is $30''$ (0.5 kpc) at $P.A. = 142^\circ$ (Elmegreen, Chromey, & Johnson 1995). The observed gas distribution, however, does not show twin peaks and/or gas ridges at the bar's leading side unlike many barred galaxies. The nuclear bar may have too small a quadrupole moment to create those features or may have a deviation from bisymmetry, which causes the lopsided gas distribution.

5. Starved Nucleus

M 81 does not have much molecular gas in the galactic center. The gas mass in the central kiloparsec is $2 \times 10^6 M_\odot$, which is more than an order of magnitude smaller than the number in more gas-rich spiral galaxies (Sakamoto et al. 1999a,b). The mass fraction of molecular gas in the central kiloparsec is $M_{\text{mol}}/M_{\text{dyn}}(r \approx 500 \text{ pc}) \approx 2 \times 10^{-3}$, where missing flux is taken into account. The low fraction is in accordance with the trend that galactic nuclei with an optical spectrum indicative of an AGN tend to have a lower gas mass fraction than do galactic nuclei with an H II type spectrum (Sakamoto et al. 1999b). The 3 σ upper limit for the mass of molecular gas in the central 100 pc is $M_{\text{mol}}^{\text{nuc}} \leq 4 \times 10^5 (V/100 \text{ km s}^{-1})^{1/2} M_\odot$, where V is the CO linewidth. Thus, it appears that M 81 is starving for infalling interstellar medium.

The lack of significant CO absorption toward M 81 is consistent with its type 1 nature in the framework of the unified scheme, in the sense that the putative accretion disk or broad line region does not suffer much obscuration from surrounding material. On the other hand, the lack of CO emission at the nucleus prevented us from verifying if there is a gas torus or disk around M 81.

With the paucity of fueling molecular gas around the active nucleus, its activity may well be limited by the intermittent supply of fuel. If the AGN flares up when, for example, the closest GMC starts to interact with the nucleus, the timescale of the variability would depend on the interval between such interactions. If a bar-streaming mechanism that radially transports the nearest GMC complexes to the nucleus is at work, as was observed in NGC 5005 (Sakamoto, Baker, & Scoville 2000), then the timescale would be of the order of $M \text{ yr} \approx (100 \text{ pc}/100 \text{ km s}^{-1})$. On the other hand, if dynamical friction to the GMCs is the only mechanism that transports the clouds, then M 81 is really starving and will not get the next large supply of fuel for 10^9 – 10^{10} yrs.

Finally, we note that a $5 \times 10^6 M_\odot$ black hole, like GMCs of similar mass, takes 10^9 – 10^{10} yrs

to fall from $R \approx 300$ pc to the dynamical center through dynamical friction. Thus, if the mass of M 81 is close to the lower value in the literature, M 81 should be older than 1 Gyr or was formed at the very center of the galactic potential or both. Tighter constraints from further observation of this nearby AGN would be useful in studies of the formation and evolution of AGNs.

6. Summary

The central kiloparsec of the nearby spiral galaxy M 81 has been observed in CO ($J=1\{0$) and, at the same time, its low-luminosity AGN M 81 has been monitored in the 3 mm continuum. A search for N ILR has also been carried out for M 81. Our observations and analysis yield the following results:

1. Most of the molecular gas in the central kiloparsec is detected on a "pseudoring" or a nuclear spiral at the galactocentric radius of ≈ 500 pc. The area within 300 pc from M 81, which appears to be at the dynamical center, is devoid of CO emission, except for diffuse emission, which can not be detected with our observations. In particular, no CO emission is detected at the nucleus nor is any CO absorption detected against the continuum emission from M 81. The upper limit for the gas mass in the central 100 pc is $M_{\text{mol}}^{\text{nuc}} \leq 4 \times 10^6 (V=100 \text{ km s}^{-1})^{1/2} M_{\odot}$. The GMCs nearest to the nucleus are 300 pc away, hence the nucleus will not be fueled by them at least in the next Myr.
2. The 3 mm continuum from M 81 showed conspicuous variation; a factor of 7 in 5 months and up to 45% in 6 hrs. The intraday variation suggests ≈ 100 AU size and 10^{11} K brightness temperature for the emitting region.
3. It is pointed out that the maximum radius of the N ILR can be several times larger than the radius at which the rotation curve turns over from Keplerian to rigid-body rotation. Despite this factor, the pseudoring at $R \approx 500$ pc is too far from the nucleus to be due to the N ILR. No CO feature that can be associated with an N ILR is found in M 81.

We are grateful to NRO staff for their help during observations. The NASA Extragalactic Database was used to carry out our research.

R E F E R E N C E S

- Adler, D . S ., and Westpfahl, D . J. 1996, *A J*, 111, 735
- Bartel, N ., and Bietenholz, M . 2000, in *Astrophysical Phenomena Revealed by Space VLBI*, Eds.,
H . Hirabayashi, P . G . Edwards, and D . W . Murphy, (Sagamihara: ISAS), p17
- Bietenholz, M . F . et al. 1996, *ApJ*, 457, 604
- Bietenholz, M . F ., Bartel, N ., Rupen, M . P . 2000, *ApJ*, 532, 895
- Binney, J ., and Tremaine, S . 1987, *Galactic Dynamics*, (Princeton: Princeton University Press)
- Bower, G . A ., Wilson, A . S ., Heckman, T . M ., and Richstone, D . O . 1996, *A J*, 111, 1901
- Brouillet, N ., Kaufmann, M ., Combes, F ., Baudry, A ., and Bash, F . 1998, *A & A*, 333, 92
- Crane, P . C ., Girda, T . S ., and Carlson, J . B . 1976, *ApJ*, 203, L113
- de Bruyn, A . G ., Crane, P . C ., Price, R . M ., and Carlson, J . B . 1976, *A & A*, 46, 243
- de Vaucouleurs, G ., de Vaucouleurs, A ., Corwin, H . G ., Buta, R . J ., Paturel, G ., & Fouque, P .
1991, *Third Reference Catalogue of Bright Galaxies*, (New York: Springer Verlag)
- Devereux, N . A ., Jacoby, G ., Ciardullo, R . 1995, *A J*, 110, 1115
- Devereux, N ., Ford, H ., and Jacoby, G . 1997, *ApJ*, 481, L71
- Elmegreen, D . M ., Chromey, F . R ., and Johnson, C . O . 1995, *A J*, 110, 2102
- Filippenko, A . V ., and Sargent, W . L . W . 1988, *ApJ*, 324, 134
- Freedman, W . L . et al. 1994, *ApJ*, 427, 628
- Fukuda, H ., Wada, K ., and Habe, A . 1998 (FWH98), *MNRAS*, 295, 463
- Fukuda, H ., Habe, A ., and Wada, K . 2000 (FWH00), *ApJ*, 529, 109
- Ho, L . C ., Filippenko, A . V ., and Sargent, W . L . W . 1996, *ApJ*, 462, 183
- Ho, L . C ., Filippenko, A . V ., & Sargent, W . L . W . 1997, *ApJS*, 112, 315
- Ho, L . C ., van Dyk S . D ., Pooley, G . G ., Sramek, R . A ., and Weiler, K . W . 1999, *ApJ*, 118, 843
- Ishisaki, Y . et al. 1996, *PASJ*, 48, 237
- Iyomoto, N ., Makishima, K . 2001, *MNRAS*, 321, 767
- Liou, M ., Stein, C . 1993, *J. Comp. Phys.*, 107, 23

- Ma, C. et al. 1998, *AJ*, 116, 516
- Pellegrini, S., Cappi, M., Bassani, L., Malaguti, G., Palumbo, G. G. C., and Persic, M. 2000, *A & A*, 353, 447
- Pogge, R. W., Maoz, D., Ho, L. C., and Eracleous, M. 2000, *ApJ*, 532, 323
- Reichen, M., Kaufman, M., Blecha, A., Golay, M., and Huguenin, D. 1994, *A & AS*, 106, 523
- Reuter, H.-P., and Lesch, H. 1996, *A & A*, 310, L5
- Sage, L. J., and Westpfahl, D. J. 1991, *A & A*, 242, 371
- Sakamoto, K., Okumura, S. K., Ishizuki, S., and Scoville, N. Z. 1999a, *ApJS*, 124, 403
- Sakamoto, K., Okumura, S. K., Ishizuki, S., and Scoville, N. Z. 1999b, *ApJ*, 525, 691
- Sakamoto, K., Baker, A. J., and Scoville, N. Z. 2000, *ApJ*, 533, 149
- Scoville, N. Z., Yun, M. S., Clements, D. P., Sanders, D. B., & Walker, W. H. 1987, *ApJS*, 63, 821
- Solomon, P. M., Rivolo, A. R., Barrett, J., & Yahil, A. 1987, *ApJ*, 319, 730
- Strong, A. W. et al. 1988, *A & A*, 207, 1
- Taylor, C. L., and Wilson, C. D. 1998, *ApJ*, 494, 581
- Tully, R. B. 1988, "Nearby Galaxies Catalog", (Cambridge: Cambridge University Press)
- Wada, K., Minezaki, T., and Sakamoto, K. 1998, *ApJ*, 494, 236
- Wada, K., and Norman, C. 2001, *ApJ*, 546, 172

Table 1. Log of observations

Date	Time		H A .		t_{middle} (JD .)	Con g.	t_{cycle} m in
	Start	End	Start	End			
1999 Nov 29	18 ^h 58 ^m	25 ^h 10 ^m	1:2	5:0	2451512.42	D	30
1999 Nov 30	17 10	23 25	2:9	3.3	2451513.35	D	30
1999 Dec 27	17 24	23 25	0:9	5.1	2451540.35	D	20
2000 Jan 1	17 37	23 25	0:3	5.4	2451545.35	D	20
2000 Jan 3	16 41	23 25	1:2	5.6	2451547.34	D	20
2000 Jan 11	13 37	22 55	3:7	4.4	2451555.26	AB	20
2000 Apr 18	06 45	16 25	4:1	5.5	2451652.98	D	20
2000 Apr 29	06 06	14 25	4:1	4.2	2451663.93	D	20
2000 Apr 30	05 28	14 25	4:6	4.3	2451664.91	D	20

Note. | Observing date and time are in UT. Hour angle of M 81 is in hours. In each cycle of duration t_{cycle} , gain calibrator is observed for 3 m in; 2 m in is used to slue telescopes; and M 81 is observed for the rest.

Table 2. Flux density of M 81

t_0 (JD)	T_{obs} day	$\overline{S_{3\text{m m}}}$ Jy	$(dS_{3\text{m m}}=dt)=S_{3\text{m m}}(t_0)$ day ⁻¹		t_2 day
2451512.29	0.26	0.25	0.62	0.18	1.6
2451513.22	0.26	0.40	1.66	0.18	0.6
2451540.22	0.25	0.51	0.22	0.18	4.5
2451545.23	0.24	0.63	1.91	0.09	0.5
2451547.20	0.28	0.98	0.32	0.05	1.6
2451555.07	0.39	0.35	0.71	0.13	0.7
2451652.78	0.40	0.25	0.56	0.14	1.8
2451663.75	0.35	0.15			
2451664.73	0.37	0.21	1.37	0.19	0.7

Note. | Observations of M 81 start at time t_0 and last for the duration of T_{obs} . Mean flux density of M 81 during observations is $\overline{S_{3\text{m m}}}$, with the absolute calibration error of about 10%. Flux densities in each transit are fitted with a linear function, $S_{3\text{m m}}(t) = S_{3\text{m m}}(t_0) + \frac{dS_{3\text{m m}}}{dt}(t - t_0)$. Gain correction has been applied before fitting. No fitting was made for the data taken on JD. = 2451663, because of poor signal-to-noise ratio. The timescale t_2 is the time in which the flux density would double or become half if the linear variation held.

Table 3. Key radii in the model

M_{BH} M	R_{nt} pc	R_{NILR} pc	$\text{max}(R_{\text{NILR}})$ pc	R_{IILR} pc
10^6	17	28	84	279
10^7	37	82	137	284
10^8	82	^y	237	

Note. | Key radii in the simulations shown in Fig. 8. The model potential is eq. (14) and the pattern speed of the bar is $\Omega_{\text{bar}} = 50 \text{ km s}^{-1} \text{ kpc}^{-1}$. See text for other parameters in the model.

^yThe minimum of $\Omega = 2$ is $60 \text{ km s}^{-1} \text{ kpc}^{-1}$ and hence, strictly speaking, an NILR does not exist. However the characteristic gas feature of NILR appears at radii where $\Omega = 2 \Omega_{\text{bar}}$.

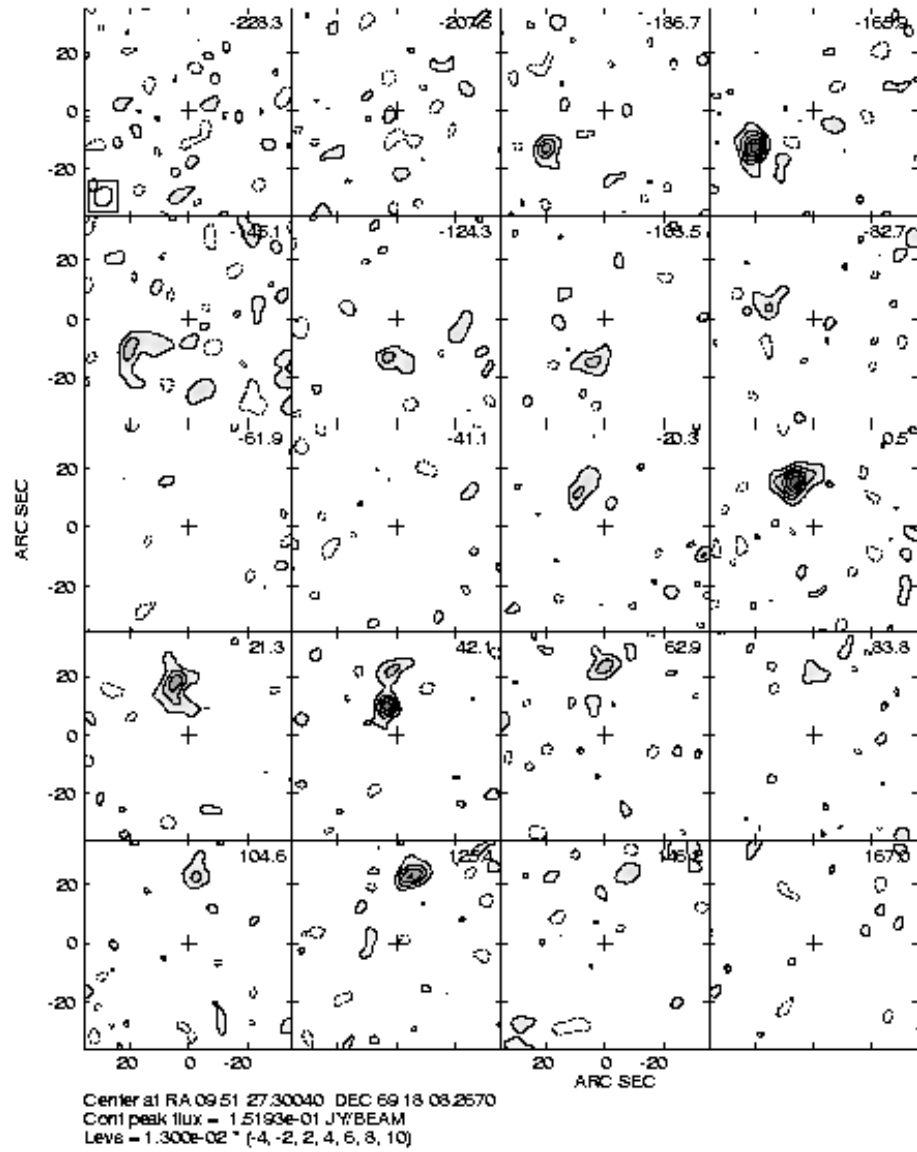


Fig. 1. CO ($J=1\{0\}$) channel maps of 20.8 km s^{-1} resolution in the central kpc of M81. Continuum emission from the nucleus (shown as a cross) has been subtracted. Contours are at 4; 2; 2; 4; 6; 8, and 10 13 mJy beam^{-1} ($= 30 \text{ mK} = 1$). LSR velocity (km s^{-1}) is shown in each panel. The synthesized beam of $6.09'' \times 5.8''$ in FWHM is shown in the bottom left corner of the first panel.

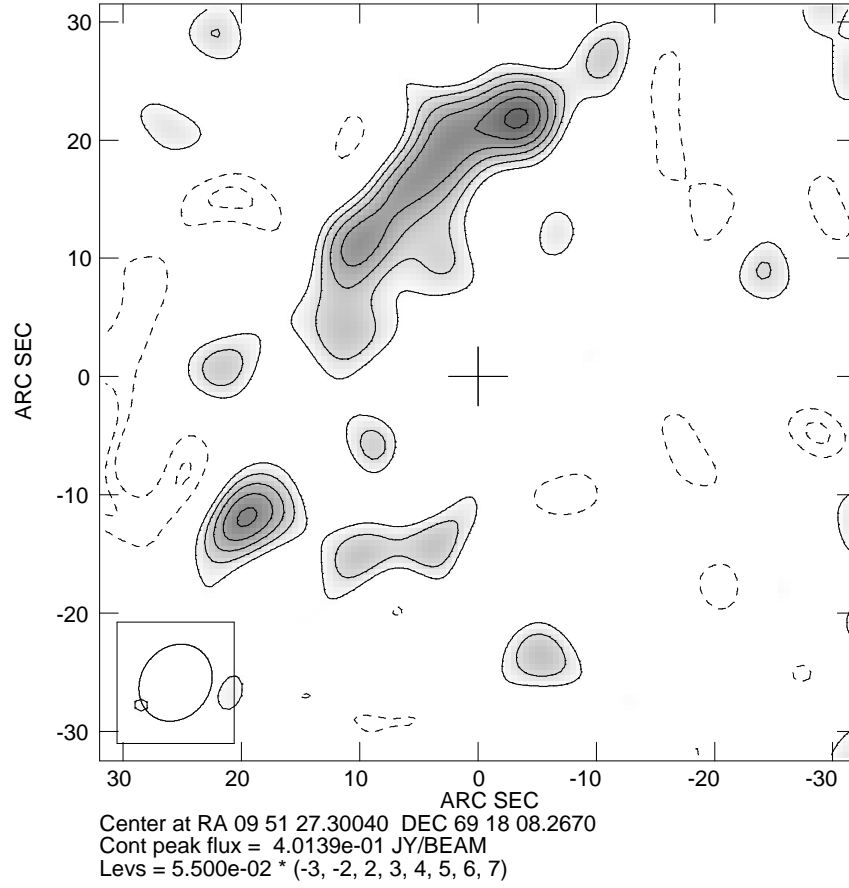


Fig. 2. Integrated intensity map of CO ($J=1\{0$) emission in the central kpc of M 81. Continuum emission from the nucleus at the position of the cross has been subtracted. Contours are at 3, 2, 2, 3, 4, 5, 6, and 7 $1.1 \text{ Jy beam}^{-1} \text{ km s}^{-1}$ (≈ 1). The contour interval and peak integrated intensity correspond to molecular gas column density of 17 and $120 \text{ M}_{\odot} \text{ pc}^{-2}$, respectively. The synthesized beam of 6.9×5.8 in FWHM is shown in the bottom left corner.

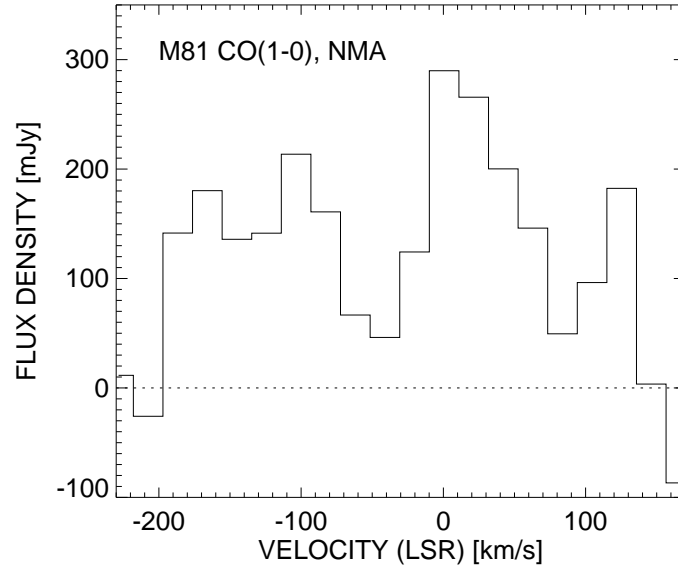


Fig. 3. Spectrum of CO ($J=1\{0$) emission in the central kpc of M 81, observed in the $1''$ (FWHM) primary beam of the NMA. The line width is 350 km s^{-1} and the detected CO flux is 50 Jy km s^{-1} , which is about half of the single-dish flux observed at the NRAO 12 m telescope. Continuum emission from the nucleus has been subtracted.

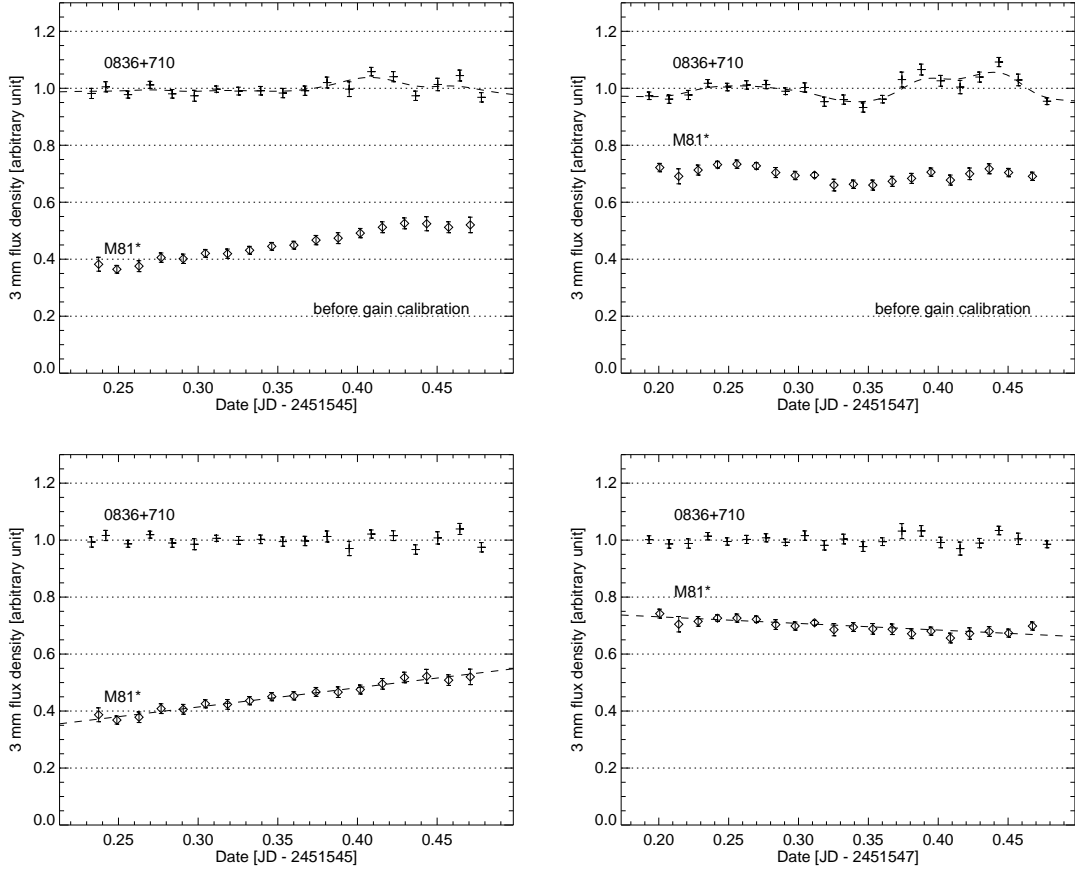


Fig. 4. Time variation of the 3 mm continuum from M 81 on JD = 2451545 (left) and 2451547 (right). Top panels show data after chopper-wheel correction and before gain calibration. Gain curves (shown as dotted lines) are derived by smoothing amplitudes of B 0836+710 with a Gaussian kernel having $\sigma = 0.015$ day and a cutoff at $t = 0.050$ day. The large gain variation in the right panel, on JD = 2451547, is most likely due to coherence loss. Bottom panels show data after applying the gain calibration. A linear fit of M 81 is plotted over the calibrated data. The monotonic variation of M 81 is clearly seen. Error bars are 1 for 0836+710 and 2 for M 81.

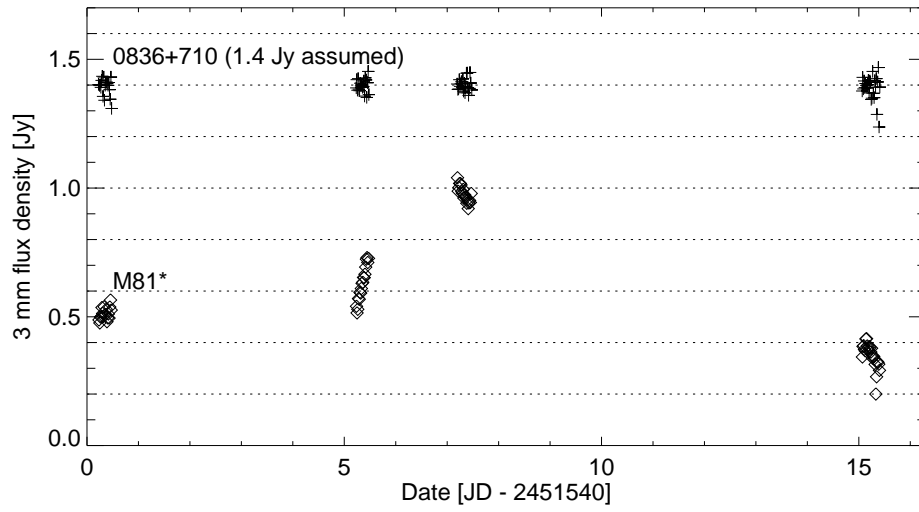


Fig. 5. Time variation of the 3 mm continuum from M81 around the flare on JD - 2451546. Instrumental gain has been calibrated assuming that 0836+710 had a constant flux density of 1.4 Jy and was unpolarized.

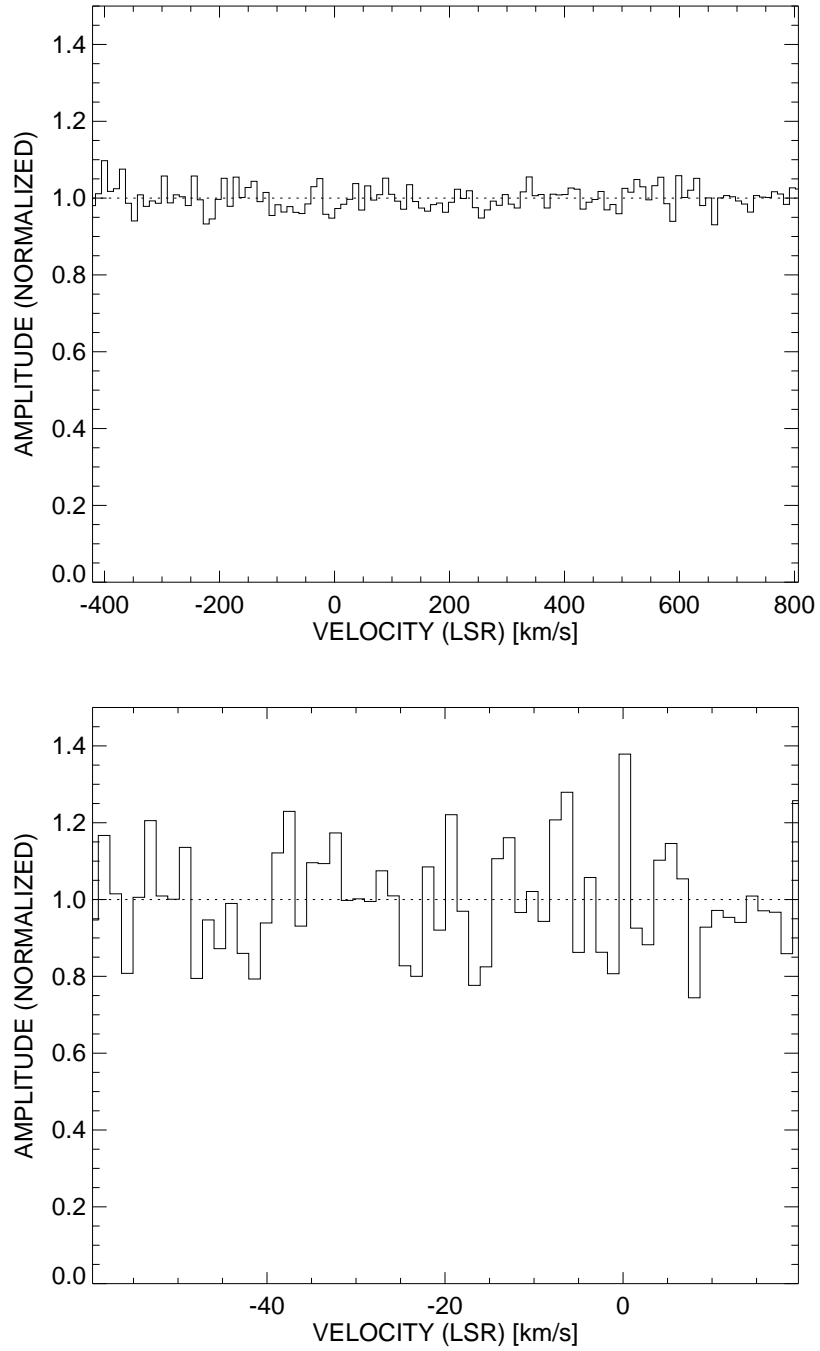


Fig. 6. Spectra of the 3 mm continuum from M 81 used to search for CO ($J=0(1)$) absorption toward the nucleus. The top panel has a 10.4 km s^{-1} resolution (obtained from UWBC), while the bottom panel has a 1.3 km s^{-1} resolution (observed with FX). A linear baseline is subtracted and amplitude is normalized to unity. The systemic velocity of M 81 is 34 km s^{-1} (LSR) and Galactic HI clouds have velocities around 3 km s^{-1} (LSR) in the direction of M 81. No absorption is seen around these velocities. The rms of the UWBC spectrum is 0.0315 and that of the FX spectrum is 0.140.

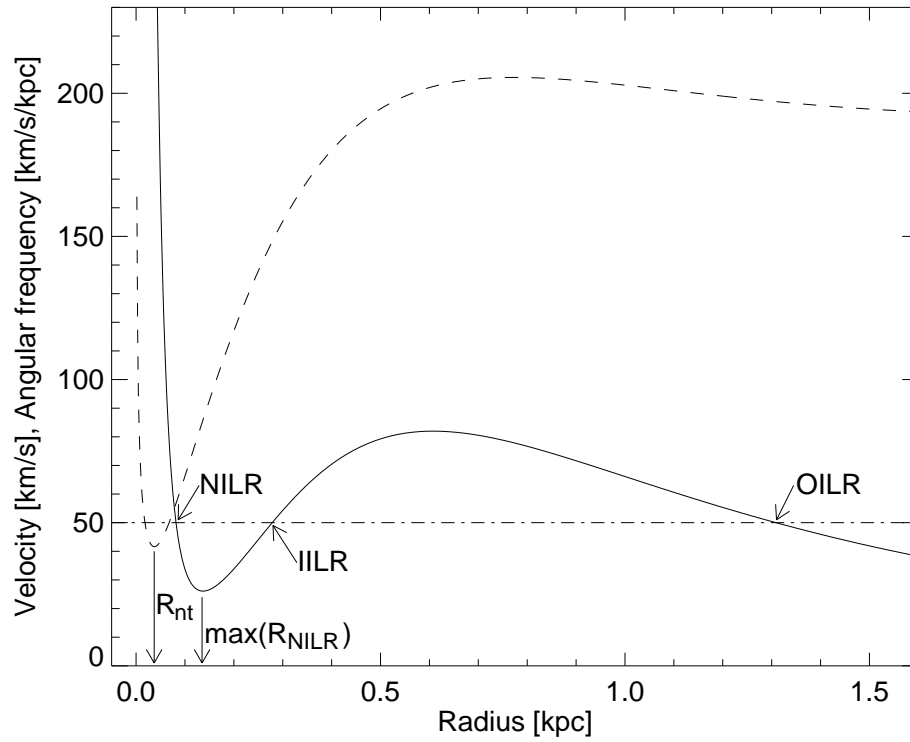


Fig. 7. The rotation curve (dashed line) and $\Omega = 2$ curve (solid line) for a model potential with a $10^7 M_\odot$ black hole at the galactic center. The minimum of the rotation curve at R_{nt} and the minimum of $\Omega = 2$ at $R = \max(R_{NILR})$ are indicated. Also marked are the nuclear inner Lindblad resonance (NILR), inner inner Lindblad resonance (IILR), and outer inner Lindblad resonance (OILR) for a bar pattern speed of $50 \text{ km s}^{-1} \text{ kpc}^{-1}$ (dot-dashed line).

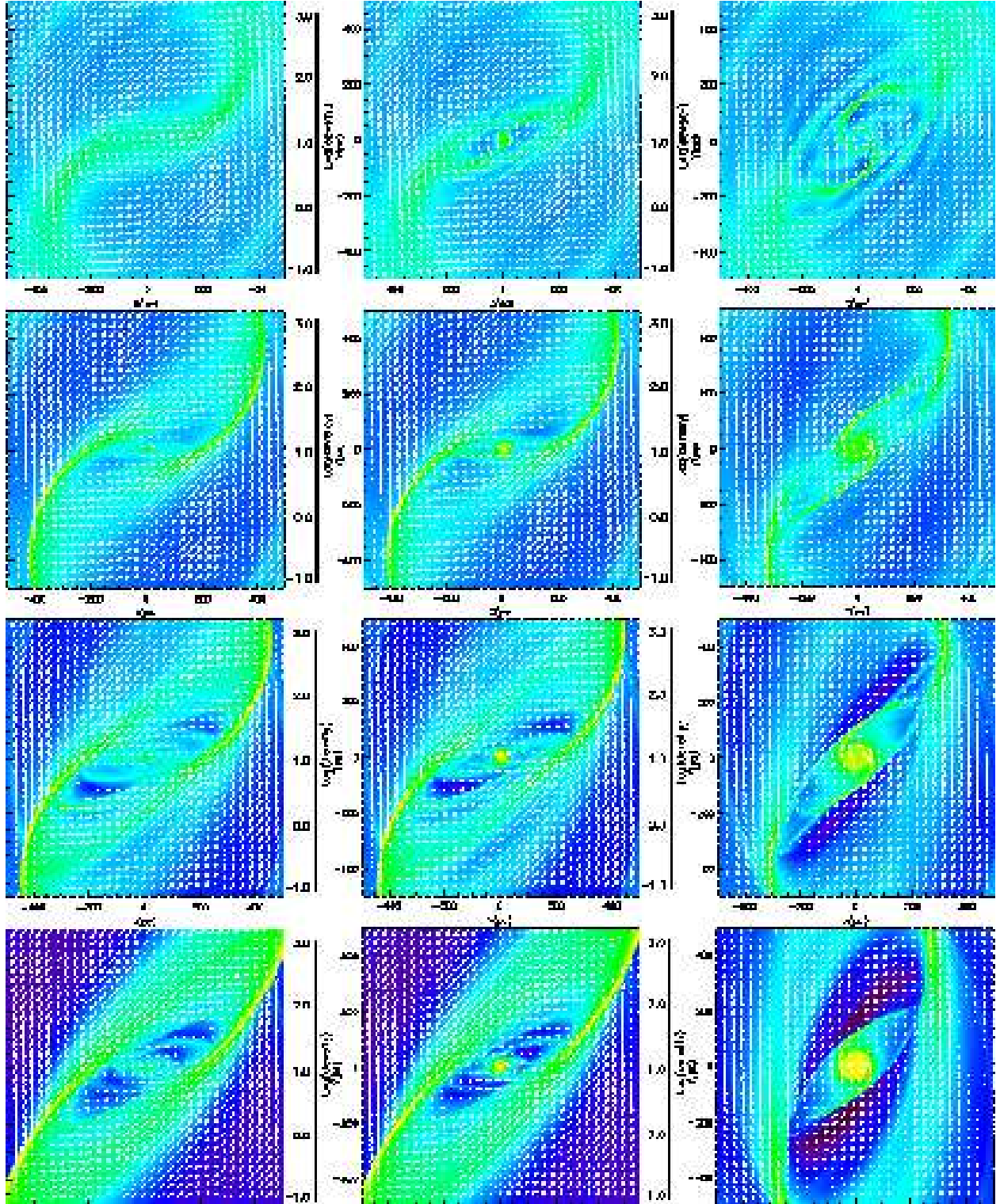


Fig. 8. Simulations of gas dynamics in the galactic center with a massive black hole and bar perturbations. Each panel shows gas surface density in pseudocolor, and gas velocities with arrows, in the frame rotating with the bar. The major axis of the bar is horizontal and the rotation of the galaxy is counterclockwise. The three columns are, from right to left, for the mass of the central black hole of 10^6 , 10^7 , and $10^8 M_\odot$ respectively. The four rows are, from the top, at $T = 20, 40, 60$, and 86 M yr. The orbital period of the system at the radius of 500 pc is 15 M yr.